Accelerated deterioration mechanism of 316L stainless steel in NaCl solution under the intermittent tribocorrosion process

Yingrui Liu [a,b], Linlin Liu [a], Shuyu Li [a,b], Rujia Wang [a,c], Peng Guo [a], Aiying Wang [a,b,*], Peiling Ke [a,b,*]

[a] *Key Laboratory of Marine Materials and Related Technologies, Zhejiang Key Laboratory of Marine Materials and Protective Technologies, Ningbo Institute of Materials Technology and Engineering, Chinese Academy of Sciences, Ningbo 315201, China*
[b] *Center of Materials Science and Optoelectronics Engineering, University of Chinese Academy of Sciences, Beijing 100049, China*
[c] *College of Chemical Engineering, Zhejiang University of Technology, Hangzhou 310014, China*

A R T I C L E   I N F O

A B S T R A C T

In this research, the tribocorrosion behavior of 316L stainless steel in simulated seawater was investigated under continuous and intermittent sliding at open circuit potential. The tribocorrosion mechanism was discussed in terms of wear morphologies, mechanical property as well as chemical composition. Meanwhile, microstructure evolution inside the wear track and open circuit potential recorded after sliding were analyzed to quantify the repassivation kinetics and evaluate the impact of the regenerated passive film on wear. The results showed that the wear rate increased under intermittent sliding when the pause time is long enough to repassivate after sliding. Repeated sliding promoted the refinement of the grain inside the sliding area, which was beneficial to the generation of the thicker and more compact passive film inside the wear track. The ruptured passive film often acted as abrasives during subsequent sliding. Therefore, the accelerated material loss under intermittent sliding was attributed to the periodic mechanical removal of the thickened passive film and the enhanced abrasive wear inside the wear track.

© 2022 Published by Elsevier Ltd on behalf of The editorial office of Journal of Materials Science & Technology.

1. Introduction

Tribocorrosion behavior is a common phenomenon and frequently observed in the engineering fields of marine explorations [1,2], food processing [3,4] and biomaterials medical implant [5–7], which is generally defined as a material degradation process resulted from the combined tribological action of relatively moving mechanical contact with corrosive chemical or electrochemical reaction [8]. Due to the intricate and not well-established synergism between the mechanical wear and electrochemical corrosion aspects, tribocorrosion is a highly complex behavior [9,10]. In this case, the tribocorrosion process not only shows significant difference compared each tribology and corrosion process separately [11], which also accelerates the material loss to a great extent [12]. Therefore, in-depth investigation of tribocorrosion behavior is particularly critical for the selection of appropriate materials applied in harsh tribocorrosion field condition.

Because of the complexity and harmfulness of this phenomenon, many investigations have been carried out to reveal the tribocorrosion mechanism and great progress has been achieved. Till now, it has been well established that material properties, wear mechanics, corrosion media properties as well as the electrochemical are the most important factors affecting the tribocorrosion resistance [1,13]. Among these, material microstructure [9,14–17], load level [18–20] and applied electrochemical potential [2,21] are the most frequently studied factors. Apparently, the tribocorrosion behavior is a highly complex issue involving many interrelated factors. More specifically, the influence of microstructure on the tribocorrosion behavior is mainly reflected in three aspects, including localized corrosion sensitivity in wear track [18], repassivation kinetics [22] and wear resistance [9] of the materials. As for the passive alloy or the coating, mechanical load always results in the deterioration of passive film in the contact area and even leads to the microstructure evolution beneath the wear track. Further, the effect of the passive film on the tribocorrosion property can be studied by using applied electrochemical potential above or below the open circuit potential(OCP) [23], which would remove or promote the formation of the passive film in wear track. Moreover, it has been reported that the depth and distribution of friction de-

formation zone beneath the wear track can also be affected by the applied electrochemical potential [17].

The above-mentioned researches provide a comprehensive perspective to the in-depth understanding of the essence of tribocorrosion conducted under constant and continuous load level within a limited test time. Considering service life, these investigations on continuous tribocorrosion cannot truly reflect the performance evolution of the materials in the actual service process. Intermittent tribocorrosion would be a better reflection of the actual working conditions of the moving components. For instance, the ball-valve fitted in the seawater pipeline [22], Implanted joint [7] as well as the plunger of seawater piston pump [24] often in an interrupted corrosion-wear state. These components suffer from static corrosion damage most of the time. Only when they are moving forward, does the tribocorrosion process occur. More importantly, some studies have revealed that the materials often exhibit quite different degradation mechanism under continuous and intermittent tribocorrosion process. Saada et al. [3] found that the wear of the 304L stainless steel (SS) used in centrifuges is clearly strengthened under the intermittent sliding which is closely related to the dominated abrasive wear mechanism. Further, surface peening processing was performed to strengthen the surface mechanical property [4], and in turn, improve the tribocorrosion resistance under intermittent sliding process. The results revealed that the nanopeened 304L SS is more sensitive to tribocorrosion under the intermittent condition than that under the continuous condition. The periodical depassivation and repassivation phenomenon were the main causes for this change. Dimah et al. [5] also studied the bio-tribocorrosion behavior of titanium biomedical alloys in different sliding modes. The results indicated that the removal of repassivated material was increased in the intermittent sliding mode and it was related to the formation of passive film during every two successive sliding processes. However, Çaha et al. [25] found that intermittency did not significantly affect the wear volume of several titanium alloys and the wear track features were not changed as well. Clearly, although some research results prove that the wear loss of material in the intermittent sliding is indeed strengthened compared with the continuous one, it does not hold true in all cases. This may be related to the passive materials or experimental parameters. At the same time, there are still few studies corresponding to this topic and the in-depth and therefore systematic study is urgently needed to understand different tribocorrosion behaviors.

Apparently, passive film exhibits a significant effect on the tribocorrosion mechanism. Accordingly, two types of electrochemical methods, OCP measurements and potentiostatic tests, were usually conducted to investigate the effect of passive film on the tribocorrosion behavior of passive alloys or coatings [26]. Potentiostatic tests often impose an constant potential on the tested samples and therefore promote the removal or formation of passive films during the sliding process, which is well suited for quantifying the contribution of wear accelerated corrosion in the total wear loss [27]. However, in practical applications the electrochemical potential depends only on the variability of the immersion experimental conditions, rather than the external imposed disturbances. Thus, the response of electrode potential is spontaneously established between the wear track and the passivated surface of the rest of the sample is a better reflection to evaluate the periodical removal and formation passive film during the sliding test [28].

Consequently, in this study, the typical and commonly used austenite stainless steel (316L SS) was assessed by the tribocorrosion behavior under the continuous and intermittent sliding modes at OCP. Specifically, intermittent sliding tests were well designed and the individual effect on sliding duration and corrosion duration as well as their synergistic contribution to the material degradation were investigated by characterizing and analyzing the mi-

crostructure evolution and the repassivation ability of the SS in detail. In that sight, it is a new attempt to get a better insight into the accelerated material degradation in intermittent tribocorrosion process. This work revealed the accelerated deterioration mechanism in the intermittent tribocorrosion process, which is beneficial to providing a more comprehensive view of scientific understanding of the tribocorrosionm behavior in practical engineering fields.

2. Experimental procedures

2.1. 316L SSs

The commercial grade austenitic 316L SS (316L SS) have been chosen as the test materials for the current investigation. The mean composition of the SS was as follows: 0.03 wt.% of C, 0.045 wt.% of P, 0.03 wt.% of S, 17.2 wt.% of Cr, 13.4 wt.% of N, 2.1 wt.% of Mo, 2 wt.% of Mn, 0.8 wt.% of Si and Fe in balance. The metallographic morphology and X-ray diffraction (XRD) spectrum (Fig. 1) show that the microstructure of 316L SS is composed of single austenite (γ-Fe) exhibiting the equiaxed grains of 10 to 30 μm in size.

The samples were machined in the form of disks of 17 mm diameter and 3 mm thickness. Then the sample surface was ground with sand-paper and finally polished with 0.5 μm diamond paste to produce the mirror like surface without scratches. Finally, the polished samples were cleaned with ethanol in an ultrasonic bath and stored in a desiccator.

2.2. Tribocorrision tests

The tribocorrision tests were performed in a linear reciprocating tribometer (Rtec, MFT5000) equipped with a three-electrode electrochemical system (ModuLab XM ECS) Fig. 2.(a) shows detailed information of the schematic of tribocorrosion apparatus.

In the present three-electrode corrosion cell, the test sample was set as a working electrode which was clamped in a self-made fixture with an exposed area of 1.96 cm². An Ag/AgCl saturated electrode was regarded as a reference electrode and a platinum was set as a counter reference. The nature aerates 3.5 wt.% NaCl solution (pH=7) at room temperature was selected as the electrolyte. All tribocorrosion tests were conducted at a normal load of 5N. The sliding velocity and stroke length were set at 0.02 m/s and 5 mm, respectively. Due to the high hardness and excellent anticorrosion properties, the polished and cleaned Al_2O_3 balls (Φ 6 mm) were selected as the counterpart. According to the Herte elastic theory [29], the normal force could produce the maximum contact pressure about 1.14 GPa at the initial sliding period, which is higher than the yield strength of 316L SS (approximately 180 MPa). Prior to the tribocorrosion tests, OCP was monitored for 1 h to stabilize the sample surface in corrosion medium. The evolution of OCP was monitored during the entire test period. The electrochemical impedance spectroscopy (EIS), conducted at OCP in the frequency range of 10^{-2} Hz–10^5 Hz with 10 mV sinusoidal perturbations, was used to evaluate the corrosion resistance of the sample before and after the tribocroorsion tests.

To investigate the effect of sliding mode on the tribocorrosion performance of 316L SS in the simulated sea environment, two types of sliding tests were carried out at OCP in this study, namely continuous sliding mode and intermittent sliding mode. The schematic representation of the tribocorrosion protocol is shown in Fig. 2(b). For the continuous sliding test (taken as control test), the total sliding time was set as 60 min. Fig. 3 shows the evolution of OCP throughout the whole continuous sliding process. As can be seen, when the sliding starts, the stable OCP of −0.13 $V_{Ag/AgCl}$ drops sharply and then plateaus at −0.38 $V_{Ag/AgCl}$. After the sliding, OCP gradually moves to positive direction. After about 15 min, OCP regains the initial stable value (−0.13 $V_{Ag/AgCl}$) before
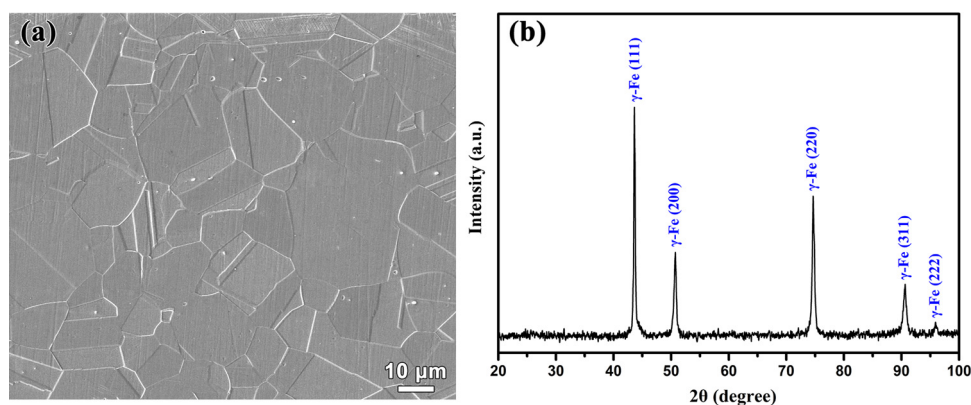
Fig. 1. (a) SEM morphology of 316L SS and (b) corresponding XRD pattern.
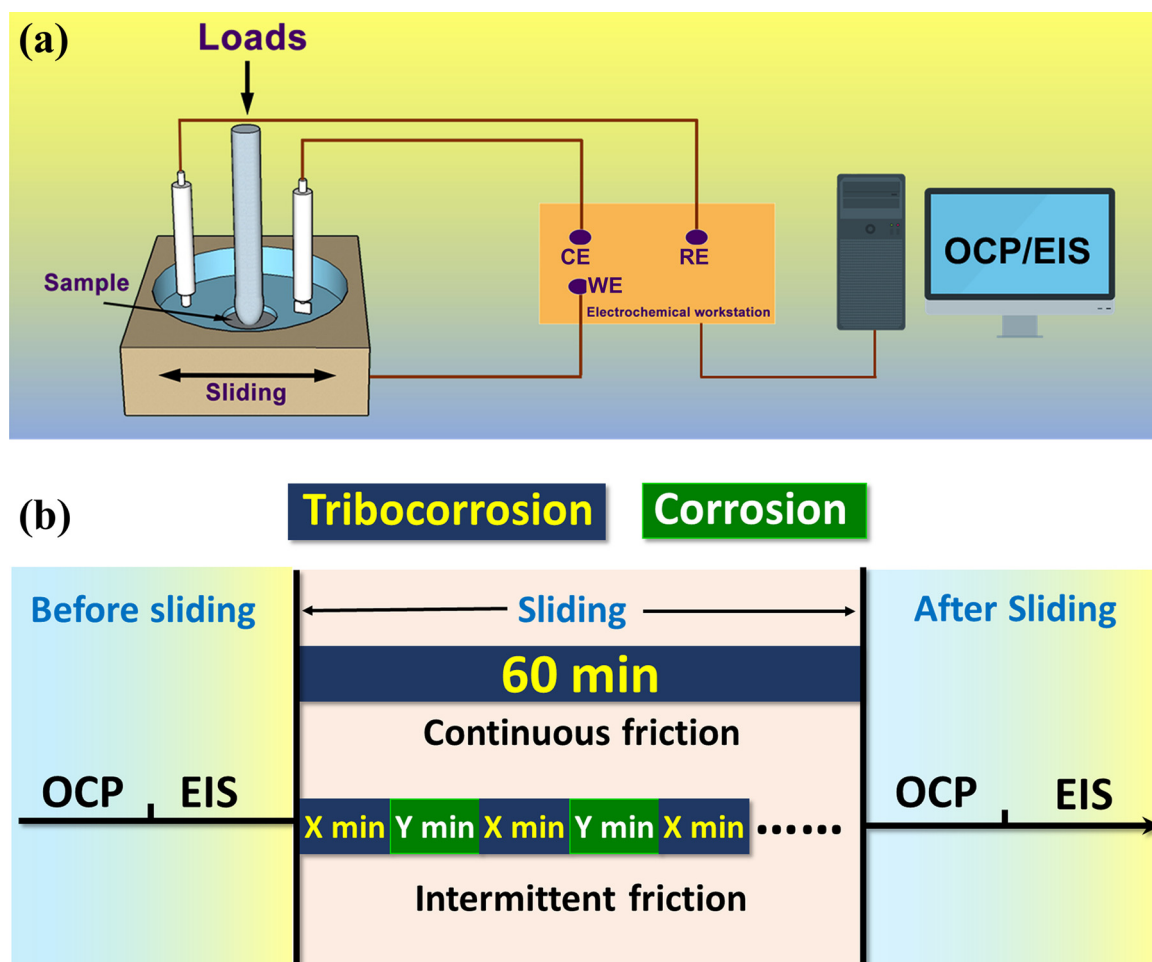

Fig. 2. (a) Schematic representation of tribometer, (b) schematic representation of the tribocorrosion protocol.

the sliding, revealing that the 15 min is a proper relaxation time to make the sample repassivated completely under the current experimental conditions. More importantly, as this duration prolongs, OCP exceeds the initial stable OCP (-0.13 $V_{Ag/AgCl}$) and eventually stabilizes in -0.1 $V_{Ag/AgCl}$. These above-mentioned results indicate that 316L SS can be repassivated after the tribocorrosion test and corrosion protection property of the reformed passive film is better than that before.

As for the intermittent sliding mode, the total sliding time was kept consistent with the continuous sliding of 60 min. In this mode, the total sliding time is made up of several short single continuous sliding processes (every single sliding duration is defined as X). Apparently, the relationship between the number of the short continuous sliding cycle (defined as n) and every single sliding duration (X) must be satisfied with condition of $n \times X = 60$. The pause duration between two successive short single continuous sliding processes is defined as corrosion time (Y). Therefore, the intermittent sliding process, in essence, consists of several tribocorrosion processes and several corrosion processes (Fig. 2(b)). According to the results from the continuous sliding mode, there is a close relationship between the pause time and the recovery of OCP, or in other words, the corrosion duration after the sliding has
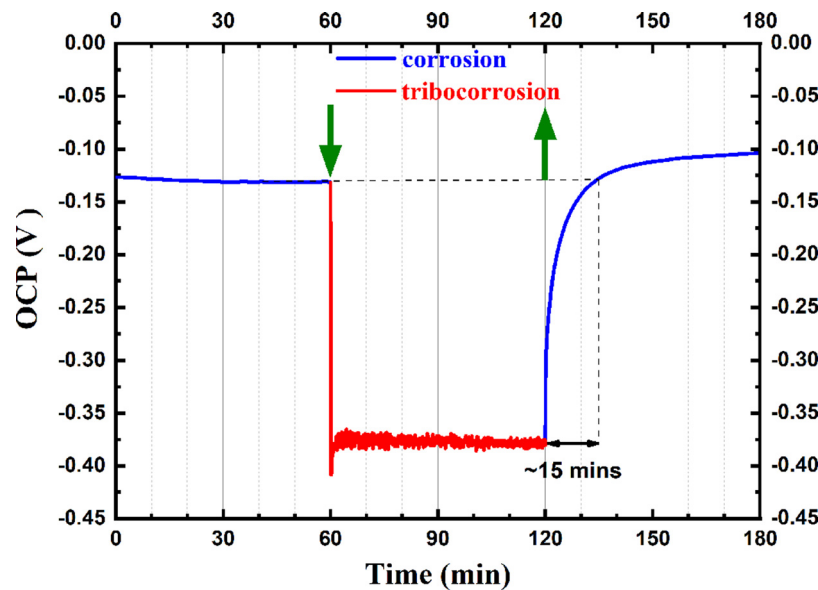
Fig. 3. Evolutions of OCP before, during and after the continuous sliding process.

an important impact on the reformation of passive film in wear track [14]. As a result, the wear volume of 316L SS during the intermittent tribocorrosion process is supposed to be interrelated to the tribocorrosion process duration (X) and corrosion process duration (Y). Accordingly, the short single continuous sliding process duration X was set to 20 min, 10 min, 5 min and 2 min, respectively. That is, the intermittent sliding process was divided into 3, 6, 12 and 30 single continuous sliding processes, respectively. Continuous sliding results indicate that OCP can be reversed to the initial stable value after ending sliding for 15 min (Fig. 3), implying that the wear track can be repassviated within 15 min under the present experimental condition. Correspondingly, the corrosion duration Y was set to 20 min, 10 min, 5 min and 2 min, respectively.

At the two test conditions, 20 min sliding−20 min pause and 20 min pause−20 min sliding are equal. Obviously, these corrosion duration settings provide a large relaxation time region from insufficient OCP recovery time to complete excess, which is helpful to understand the effect of repassivation degree on the tribocorrosion behavior. Therefore, compared with the continuous sliding mode, the tribocorrosion behavior of 316L SS in the intermittent sliding mode can be investigated in detail through changing the single continuous sliding duration X and corrosion duration Y.

2.3. Characterization of samples

The metallographic surface and cross-sectional morphologies of 316L SS were examined by using a scanning electron microscope (SEM, FEI Quanta FEG 250, USA), as well as the wear tracks after the tribocorrosion tests. The phase composite was characterized by XRD (Bruker D8 Advance, Germany) with a diffractometer by using Cu K_α radiation. The scan rate was 5°/min with the 2θ range of $20°−100°$. The subsurface microstructure evolution beneath the wear track was studied by using a transmission electron microscope (TEM, Talos F200X, USA). TEM samples of the cross-sectional profiles of the wear track were performed by the focused ion beam technique (FIB, Carl Zeiss Auriga Germany). After the tribocorrosion tests, the wear volume loss was calculated for all conditions according to the method reported in literature [30]. The profile of the wear track was quantified by measuring the profiles across the wear track with a surface profilometer (Alpha-Step IQ, KLA-tencor, SUA). The micro-hardness and elastic modulus of the sample were measured both inside and outside the wear tracks

using a nanoindenter (Nano Indenter, MTS Ltd, USA). X-ray spectroscopy (XPS, Thermo Scientific ESCALAB 250) depth profiles were carried to analyze the distribution of chemical compositions in the reformed passive film in wear tracks. The sample's surface was sputtered by using an argon ion gun operating at 5 keV to conduct in-depth profile analysis of the passive film. The argon ion beam with a current density of ∼100 μA/cm^2 was used to etch a 1.5 mm × 1.5 mm selected area. The spectra were collected for the typical elements existing in the oxide film of 316L SS: oxygen (O 1s), iron (Fe 2p), carbon (C 1s), nickel (Ni 2p), chromium (Cr 2p), molybdenum (Mo 2p). After the etch test, all XPS spectra were analyzed by using CasaXPS analytic software and the peak position of the core spectra was calibrated by the C1s peak with a binding energy of 284.6 eV.

3. Results

3.1. Evolutions of OCP and wear rate in intermittent tribocorrosion process

3.1.1. The effect of single sliding time X on OCP and wear rate evolution

OCP monitoring provides the immediate information about the chemical state inside the wear track. The evolutions of OCP before, during and after sliding test with different sliding time (X) are shown in Fig. 4. Here, the pause duration (corrosion time Y) was set as a constant of 20 min while the single sliding time X changed within a wide range, which varied from 20 min to 2 min. Apparently, as the single sliding time X decreases, the number of short continuous sliding cycles n increases dramatically. For instance, when the sliding time was the minimum value of 2 min (Fig. 4(d)), the maximum sliding cycles n of 30 is reached. At the same time, the total test time sharply increases as well. Before the initiation of the sliding, the alloy surface was kept passive state since OCP value maintained constant at about −0.12 $V_{Ag/AgCl}$. Once the sliding starts, OCP rapidly shifted to the negative direction and then plateaued at about −0.38 $V_{Ag/AgCl}$. When the sliding ceased, OCP gradually rose up to exceed the initial level and finally achieved a quasi-steady state of about from -0.05 $V_{Ag/AgCl}$ to -0.06 $V_{Ag/AgCl}$, which showed similar variation characteristics compared with the continuous tribocorrosion test result as displayed in Fig. 3. Consequently, as is clearly seen the variation of sliding time
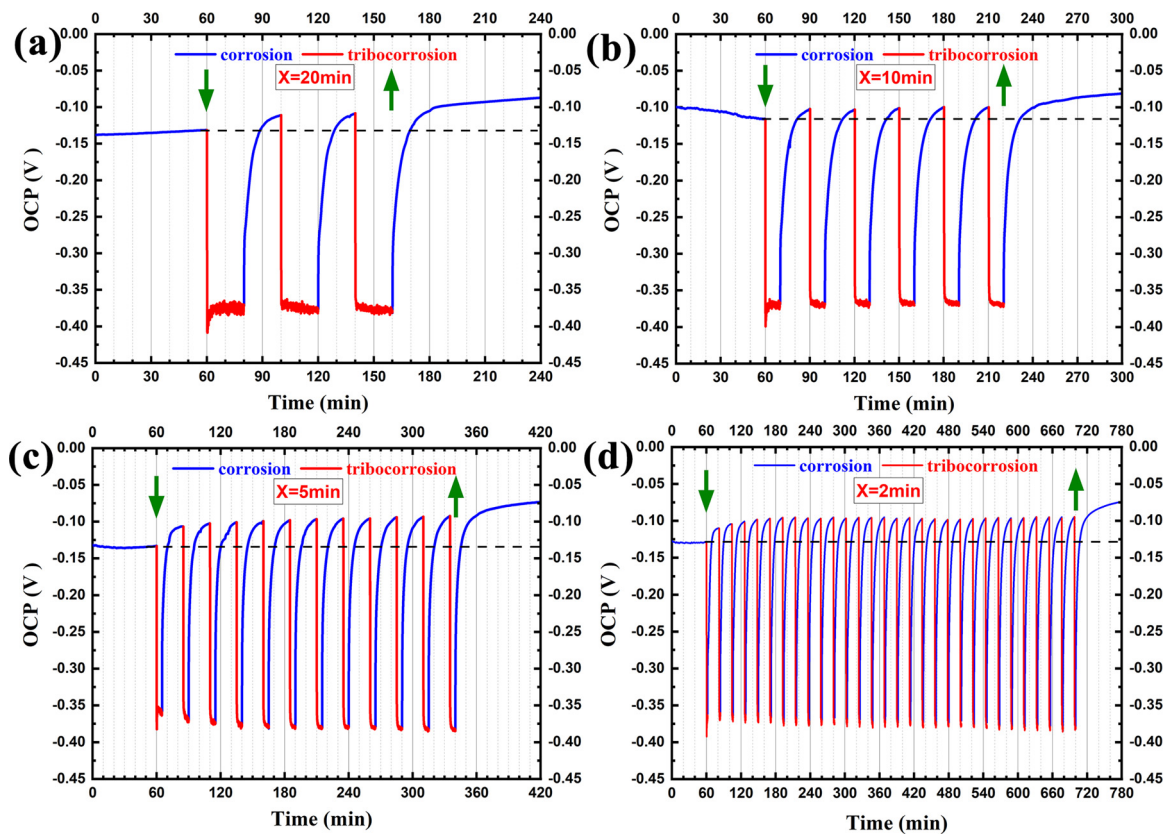
Fig. 4. Variations of OCP with time recorded before, during and after sliding in intermittent mode with fixed duration time $Y = 20$ min and the varying sliding times X. (a) $X = 20$ min, (b) $X = 10$ min, (c) $X = 5$ min and (d) $X = 2$ min.
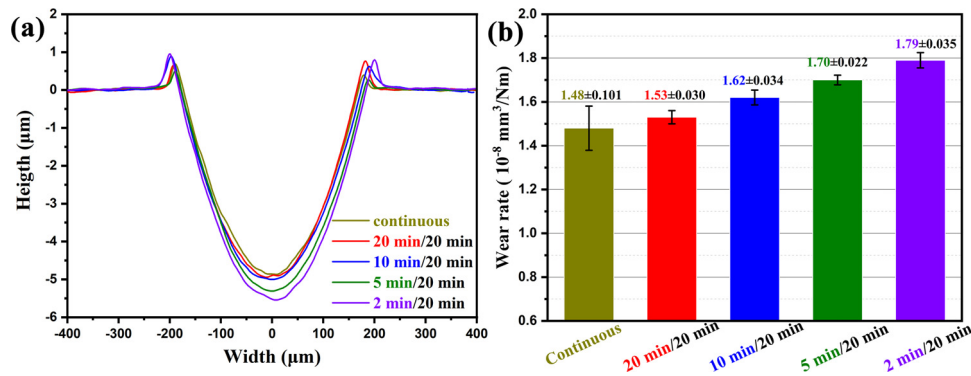

Fig. 5. Cross-sectional profiles of the wear track under continues friction and intermittent friction for varying tribocorrosion time X (a), corresponding calculated wear rate (b).

X did not affect OCP evolution when the pause time is fixed at a constant of 20 min, indicating that the repassivation completely occurred within the given pause time of 20 min. After the sliding tests, all OCP values exceeded the initial level, which is thus called "transpassivation behavior". This phenomenon is closely related to the reformed passive film in wear track after sliding tests. The variation of OCP provides the information regarding the surface electrochemistry state of the tested sample, and thus the transpassivation phenomenon indicates the modified surface state in the wear track.

After the intermittent sliding tests, the wear track profiles were measured to calculate the wear rate and the results are shown in Fig. 5. As can be seen from Fig. 5(a), the cross-sectional profiles area of continuous sliding presents the lowest value and the areas obtained from the intermittent sliding mode increase with

decreasing the single sliding time X. Fig. 5(b) clearly shows that the wear rate increases as the sliding cycle increases. This means that the wear loss depends on the multiple periodic removal of the sample, that is, the more sliding cycles are conducted, the higher wear rate is produced. All the wear rates calculated from the intermittent sliding mode are larger than those from continuous one, which showed the accelerated deteriorated tribocorrosion resistance under the intermittent condition.

3.1.2. The effect of pause time Y on OCP and wear rate evolution

Further, the evolutions of OCP collected during the different pause time (Y) while with the fixed sliding time ($X = 2$ min) are recorded and the results are shown in Fig. 6. Apparently, OCP variation trend is consistent with that mentioned previously. That is, the periodic fluctuation of OCP is presented with the load appli-
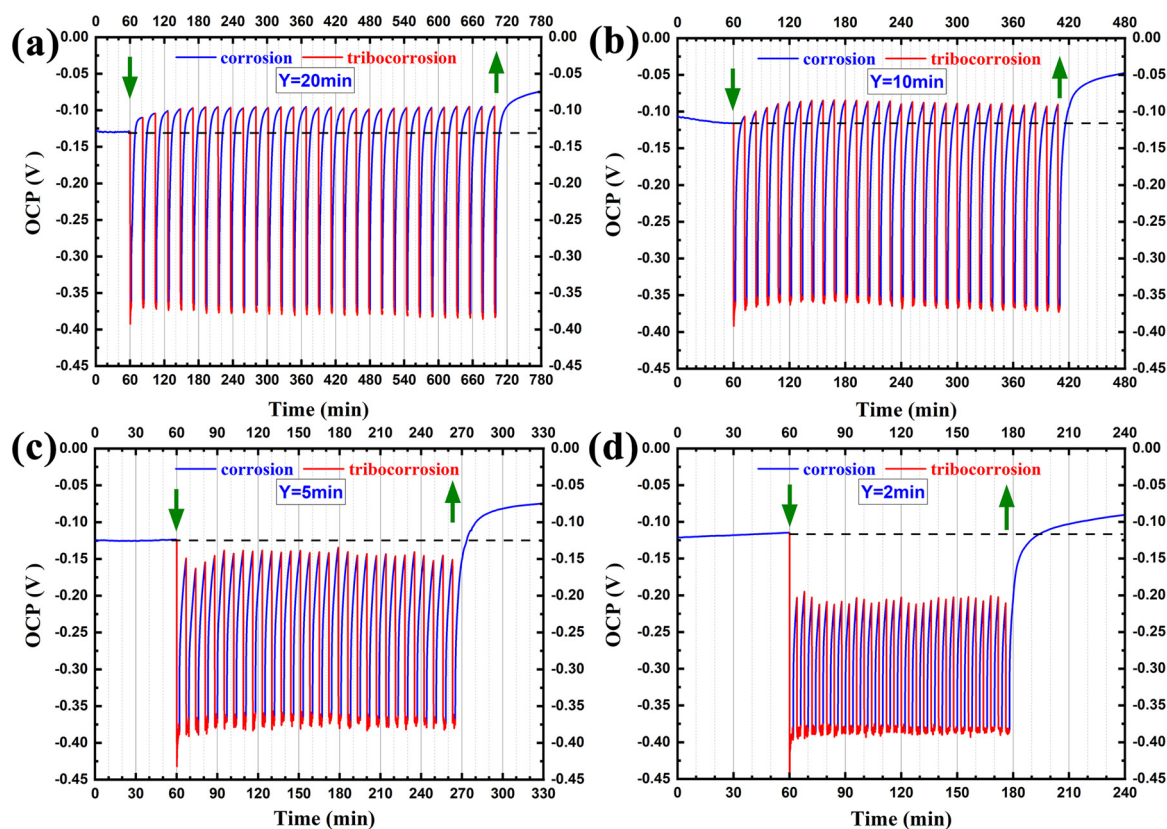
Fig. 6. Variations of OCP with time recorded before, during and after sliding under intermittent mode with fixed sliding time $X = 2$ min and the varying pause times Y. (a) $Y = 20$ min, (b) $Y = 10$ min, (c) $Y = 5$ min and (d) $Y = 2$ min.

cation and unloading as a fast response to the passive film local removal. As can be seen, the recovered OCP value gradually decreases with shortening the pause time from 20 min to 2 min. However, the recovery of OCP is dependent on the pause duration. When the pause time is higher than 10 min, the wear track can be completed repassivated since the recovered OCP is higher than that of initial value, exhibiting typical transpassivation phenomenon. When the pause time is reduced to 5 min or even shorter, OCP cannot be recovered to the initial state before the next sliding begins. This result indicates that the denser and compact passive film in wear track cannot be formed within a shorter pause duration after the sliding tests. More importantly, the time required for OCP recovery to the initial stable value in the intermittent sliding mode is much shorter than that in continuous sliding mode (approximately 15 min in Fig. 3), demonstrating that the periodic sliding changes the repassivation kinetics of formation of passive film in wear track. The results mentioned above indicate that the pause duration has a significant effect on the repassivation behavior of 316L SS after the sliding tests.

The wear rate is also calculated after measuring the cross-sectional track profile and the results are shown in Fig. 7. Clearly, the cross-sectional profile area decreases with shortening the pause duration from 20 min to 2 min (Fig. 7(a)), implying that the wear loss is gradually decreased. Moreover, the depth and width of the track is closely related to the pause duration between the two successive sliding tests. Specifically, if the pause time is too short to make the wear track repassivated completely ($Y = 2$ min and 5 min), the cross-sectional profile is relatively narrow and shallow. On the contrary, if the pause duration is sufficient ($Y = 10$ min and 20 min), the profile is wider and deeper, representing a relative higher wear loss in the current situation. Consequently, the calculated wear rate (Fig. 7(b)) shows that the sample of 2 min/20 min

presents the largest wear rate compared with the others, which is consistent with the results obtained from Fig. 5. This result indicates that when the number of sliding cycles is fixed at 30, the wear rate is tightly associated with the repassivation level of wear track after sliding process; namely, the completed repassivated wear track causes the most serious wear loss while the partial repassivated wear track results in lighter wear loss.

3.2. Microstructure and phase transformation inside the wear track

The transpassivation phenomenon (Fig. 4) above also indicates that the sliding process has changed the electrochemical state within the wear track under the current experimental condition. Therefore, cross-sectional images underneath the wear track after intermittent sliding (2 min/20 min) are characterized by SEM and TEM, as shown in Figs. 8 and 9.

Although the low-magnification image (Fig. 8(a)) only shows the indistinct wear track profile, the enlarged image (Fig. 8(b)) clearly presents a very thin (about 2,3 μm) deformation layer formed at the outermost surface (Fig. 8(a)) as well as some stripes which are also located close to the surface of the wear track, indicating the twin deformation induced by frictional shear force. Apparently, the thickness of the deformation layer is not homogeneous, which is various from grain to grain. Beside, it seems that the deformation was confined within the grains located at the surface. Moreover, the grain boundaries do not reach the surface of wear track but ends at the edge of the inner deformation layer. These results therefore indicate that when the harder Al_2O_3 counterpart slides cross 316L SS, the relatively softer surface will undergo the plastic deformation and generate the twins within the contact grains. In order to investigate phase transformation mechanism in depth, bright field TEM images combined with selected
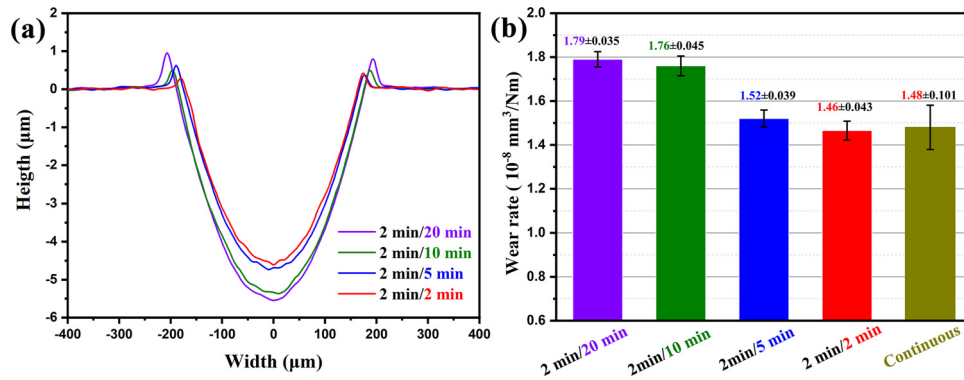
Fig. 7. Cross-sectional profiles of the wear track under continues friction and intermittent friction for varying tribocorrosion time X (a), corresponding calculated wear rate (b).
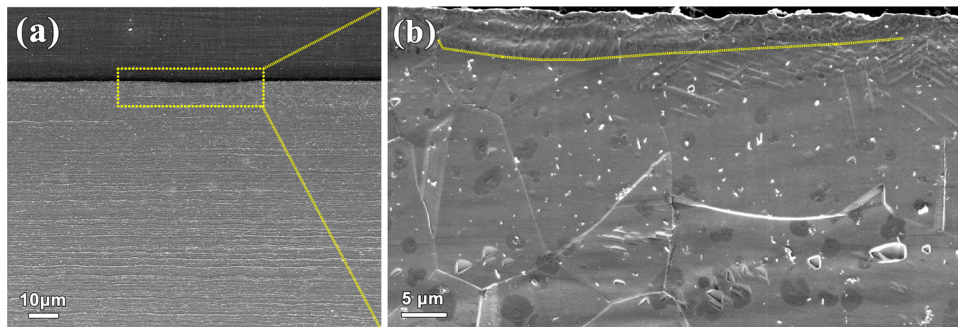

Fig. 8. Cross-sectional morphology of wear track after tribocorrosion test (a) and locally enlarged view (b).

area electron diffraction (SAED), as well as high-resolution TEM (HRTEM) were adopted, as can be seen from Fig. 9.

The microstructure image underneath the wear track within 1,2 μm presents a clear delamination phenomenon, as presented in Fig. 9(a). Local enlarged images obtained from two typical areas of A and B positions present that the surface deformation layer is characterized by a lot of parallel strips with a preferred orientation and combined with the width of 100–200 nm (Fig. 9(b)), but below the deformed layer it exhibits a typical fine equiaxed crystal (Fig. 9(c)). Further, the concentric diffraction rings in SAED (Fig. 9(d)) and the crystal plane spacing measured from HRTEM images (Fig. 9(e) and (f) which from A position) prove the initial γ-austenite phases have transferred to the α'-martensite after the wear, indicating that these strips phases belong to lath martensite. Below the deformation region, SEAD (Fig. 9(g)) and HRTEM results (Fig. 9(h) and (i)) obtained from B position demonstrate that the dominant phases in this area are α'-martensite but some initial γ-austenite phases are still found. Clearly, phase transformation induced by the sheer force occurs under the wear track, which can be related to the transformation mechanism as follows [9]: γ-Fe (austenite)-twining- α'-Fe (martensite).

3.3. Hardening effect inside the wear track

The evolution of microhardness inside and outside the wear track after intermittent sliding test (2 min/20 min) were evaluated by using nanoindentation experiment as shown in Fig. 10.

In general, under a certain load, the smaller the indentation depth is, the harder the material is. Apparently, the strain hardening occurs after the tribocorrosion test because of the increased hardness inside the wear track. The microhardness increases from the initial value of 4.22 $\pm$ 0.6 GPa to 6.82 $\pm$ 0.6 GPa, showing a 61.5% increase after the sliding process. Beside, the elastic modulus increases as well. It is noted that the grain refinement and

phase transformation have occurred within the wear contract area, which indicates that the applied load produced a significant microstructure evolution. The increased densities of grain boundaries and dislocations blocked the dislocation movement, thus leading to higher hardness. This therefore causes the wear contact area to yield higher microhardness compared with the unworn area.

3.4. Surface passive film composition

XPS depth profile analysis was conducted to investigate the passive film composition. Fig. 11 shows the element depth profiles collected inside (Fig. 11(a)) and outside (Fig. 11(b)) the wear track after the intermittent tribocorrosion tests. The results indicate that the surface passive film inside the wear track is thicker than that outside the wear track. That is, after the sliding the repassivation kinetic inside the wear track has changed, illustrating a surface electrochemical state transformation induced by the repetitive wear process. Consequently, the re-growth of the passive film inside the wear track was promoted as compared with the surrounding passivated area.

3.5. EIS results

Fig. 12 presents EIS plots and fitting results before and after the intermittent tribocorrosion tests. Fig. 12(a) shows Nyqiust plots of the sample, which exhibits an approximate quarter capacitance loop over the test frequency range. However, the capacitive loop diameters of the sample after sliding were slightly larger than those before sliding, indicating an improved corrosion resistance after the tribocorrosion test as the diameter is positively correlated to the polarization resistance [26]. Beside, Bode plots also provide abundant information about the electrochemical responses. Fig. 12(b) shows that the absolute impedance value |Z| becomes higher after the sliding, indicating a better corrosion re-
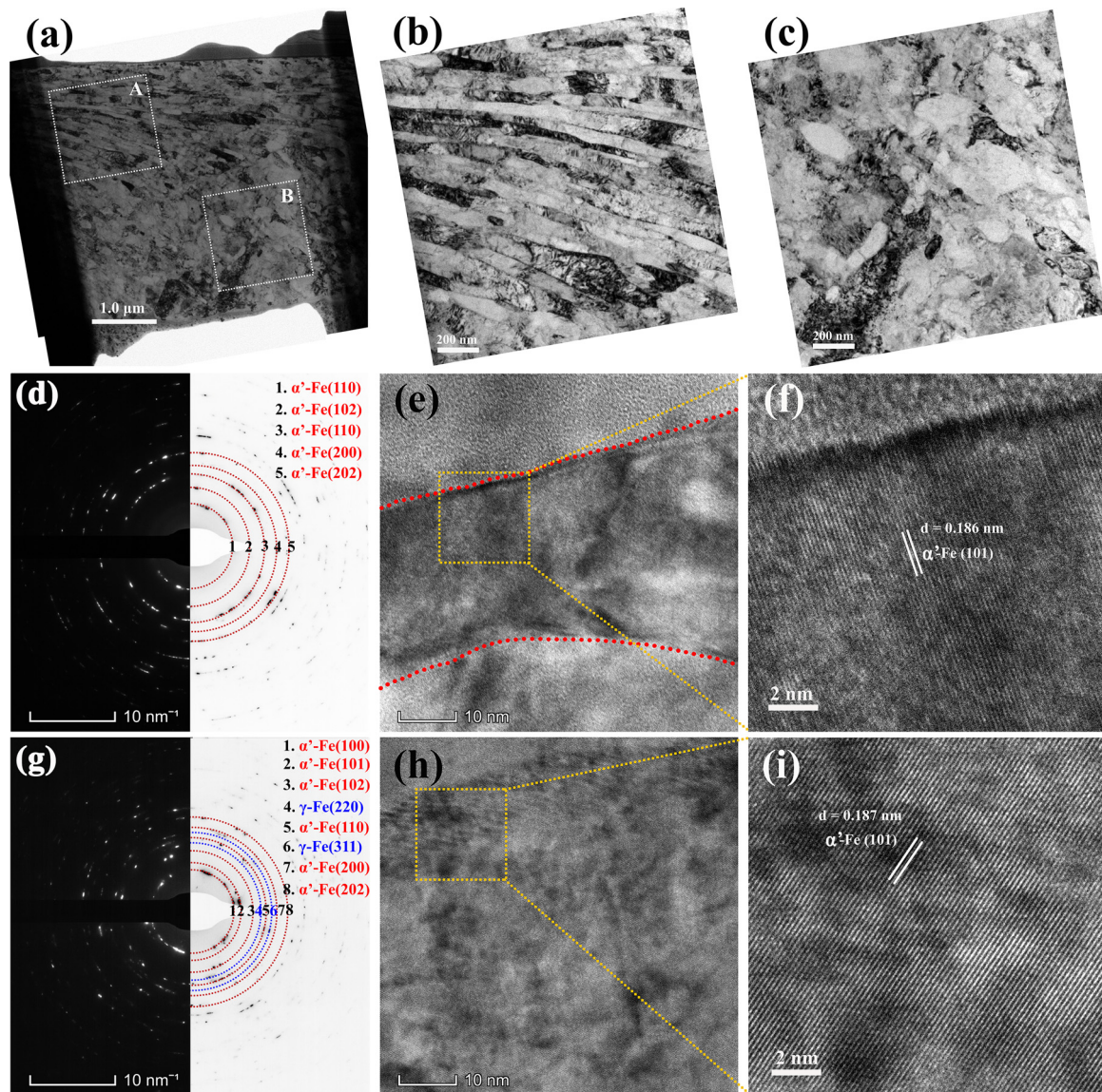
Fig. 9. Characterization of microstructures beneath wear track after tribocorrosion test: (a) overall view of BFTEM image, (b) locally enlarged BF image obtained in A position, (c) locally enlarged BF image obtained in B position, (c)–(f) SAED pattern and HRTEM images of A position, (g)–(i) SAED pattern and HRTEM images of B position.

sistance after the sliding possesses. Moreover, frequency-phase plot (Fig. 12(c)) proves that after sliding, the sample proposes a higher phase angle at low frequency range (10^{-2} Hz–10^{-1} Hz), demonstrating that the repassivated surface has better protection performance. In summary, EIS results demonstrate that the repassivated wear track after sliding possesses a better corrosion resistance.

Further, in order to quantitatively study the effect of sliding on the corrosion resistance, all EIS results were fitted with an equivalent circuit with two defined time constants (Fig.12(d)). A constant phase element (CPE) was introduced in this circuit to model the "scattering effect" resulting from the non-homogeneous nature of the surface [31]. The impedance of CPE is described as follows:

$$Z_{CPE} = Y^{-1}(j2\pi f)^n \tag{1}$$

where j is the imaginary unit, f is the frequency. Y is the magnitude of CPE. n is the parameters associated with CPE. The better capacitive response is dependent on how close n is to 1. That is, if n is approximately equal to 1, the parameter of Y can be converted into a pure capacitance. In this circuit, R_s presents the solution resistance, CPE_f and R_f are the impedance and capacitance of the passive film formed on the surface, R_{ct} and CPE_{dll} are associated

Table 1
Fitting parameter values for EIS spectra of 316L SS before and after sliding.

Parameters	Before sliding	After sliding
R_s ($\Omega \bullet cm^2$)	14.9	11.1
Y_f ($\Omega^{-1}cm^{-2}n^{-2} \times 10^{-5}$)	3.57	0.21
n_f	0.916	0.818
R_f ($M\Omega \bullet cm^2$)	2.82	2.16
Y_{dll} ($\Omega^{-1}cm^{-2}n^{-2} \times 10^{-5}$)	1.71	2.78
n_{dll}	0.719	0.931
R_{ct} ($M\Omega \bullet cm^2$)	0.61	1.15
$\chi^2 \times 10^{-4}$	5.93	3.95

with the impedance and capacitance of the double layer. The fitting results are shown with solid lines and are in good agreement with the experimental results, which can also be reflected by the small χ^2 values. All the fitting parameters are listed in Table 1. As can be seen, the electron transfer resistance (R_{ct}) clearly increases from 0.612 M$\Omega \bullet cm^2$ to 1.15 M$\Omega \bullet cm^2$ after sliding, presenting an enhanced resistance of 46.7% in static corrosion condition. The in-
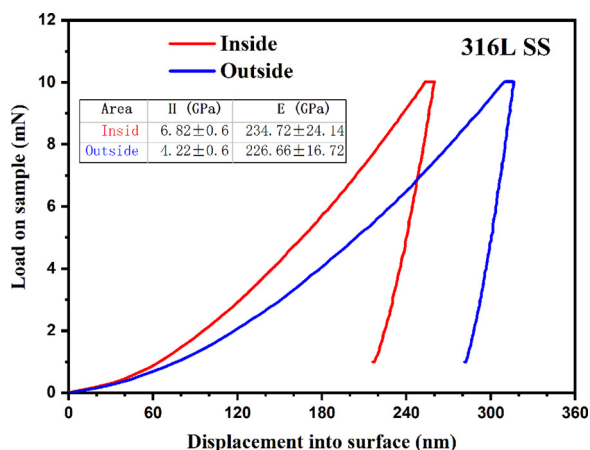
Fig. 10. Indentation curves inside and outside of the wear track after tirbocorrosion test. The average calculated hardness and elastic modulus values are inserted.

crease of R_{ct} indicates the improved repair capability of passive film inside the wear track.

4. Discussion

4.1. The repassivation behavior at different intermittent configurations

The excellent anti-corrosion performance of 316L SS contributes to the spontaneously formed passive film on the surface, which provides a barrier between external environment and active metal and therefore prevents the active dissolution of metals. The passivation ability mainly depends on the material chemistry (Cr content and its distribution) and characteristics of the corrosion solution [32,33]. During the tribocorrosion tests, when the sliding starts, the passivated surface is broken and the base materials are exposed. At the end of sliding, the new passive film is formed within a short time quickly and limits further corrosion dissolution of material inside the wear track. In tribocorrosion, the local abrasion of passive film during sliding and the re-growth of which after sliding in the contact area can be investigated by the electrochemical techniques along with the test [26,34]. This dynamic state can be described by OCP technique, which is the potential formed between the tested metal sample and the electrolyte spontaneously. The evolution of OCP can be interpreted by a simple galvanic coupling model during the tribocorrosion process [28]. In this model, the galvanic potential is a mixed potential reflecting the surface state of the depassivated worn area and the surrounding passivated surface. Therefore, the shift of the galvanic potential can be significantly affected by the removal of passive film induced

by the sliding process. Apparently, the respective intrinsic potential of the materials, the ratio of worn and unworn areas as well as their relative position and kinetics of anodic and cathodic reaction are critical parameters which influence OCP evolution during the tribocorrosion [26]. Therefore, the depassivation and repassivation behavior can be analyzed by investigating OCP evolution. In this case, the cathodic shift of OCP observed in Figs. 4 and 6 can be explained by the galvanic potential established between the inside wear track (as cathodic) and outside wear track (as anodic). As can be seen from the two figures, the rates at which OPC decreases when the load is applied and increases when unloaded are quite different, indicating that both underlying processes and kinetic are different. The sudden decrease of OCP is due to the mechanical destruction of passive film while the slow increase is attributed to the re-establishment of passive film inside the wear track. Beside, it should be noticed that the cathodic shift degree of OCP at the fist sliding cycle is presented with a more intense decrease of potential and then followed by gradual increase to a stable value, which is quite different from the other following sliding cycles during the intermittent tribocorrosion. Except for the first sliding cycle, the rest of those present similar and stable cathodic shift (-0.37 $V_{Ag/AgCl}$) through the whole test, indicating that the kinetic inside the wear track has changed at the first sliding cycle. Evidently, the change of kinetic inside the wear track not only affects the cathodic shift degree of OCP but also influences the required repassivation time after sliding. Here, the recovery time required from the stable tribocorrosion potential to the initial level is defined as repassivation time. It can be clearly seen from the continuous tribocorrosion (Fig. 3) and intermittent tribocorrosion (Fig. 4) that the increase trend of OCP after sliding presents typical logarithmic rule, if the pause duration provided is sufficient to make the wear track repassivated completely. Moreover, Fig. 4 shows that the repassivation time obtained from the intermittent sliding is shorter than that of the continuous sliding (Fig. 3), indicating that repassivation time can be affected by the intermittent configurations. A local enlarged draw from Fig. 3 is shown in Fig. 13(a), which presents typical increase of OCP with a certain time. The repassivation rate after sliding can be calculated by the inserted equation which was reported in Hanawa et al. [35]

$$\Delta E = k_1 \log t + k_2 \qquad (2)$$

where ΔE is the potential variation, $t(s)$ is the time after the sliding, k_1 is the slope and k_2 is a constant determined by the kind of corrosive media. The ΔE is fitted according to the measured values within the repassivation time. The measured repassivation time and the fitted repassviation rate (k_1) are shown in Fig. 13(b). Clearly, there is an opposite relationship between the repassivation time and repassivation rate (k_1). With the increase of single sliding duration (X), k_1 fitted from intermittent sliding mode increases
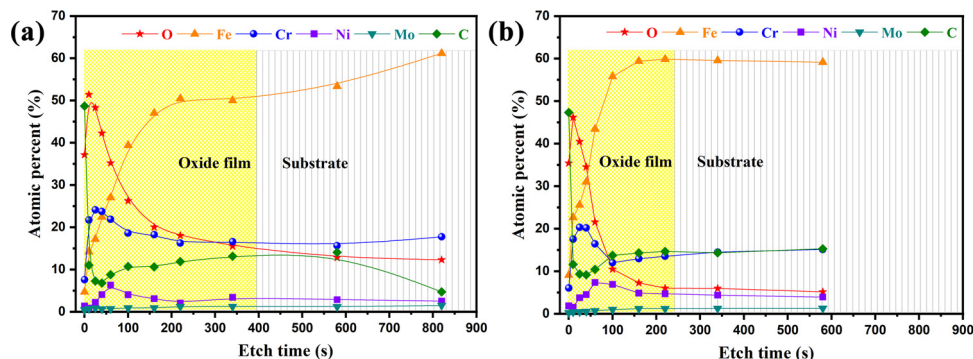

Fig. 11. XPS depth profiles measured after the tribocorrosion test, (a) inside of the wear track, (b) outside of the wear track.
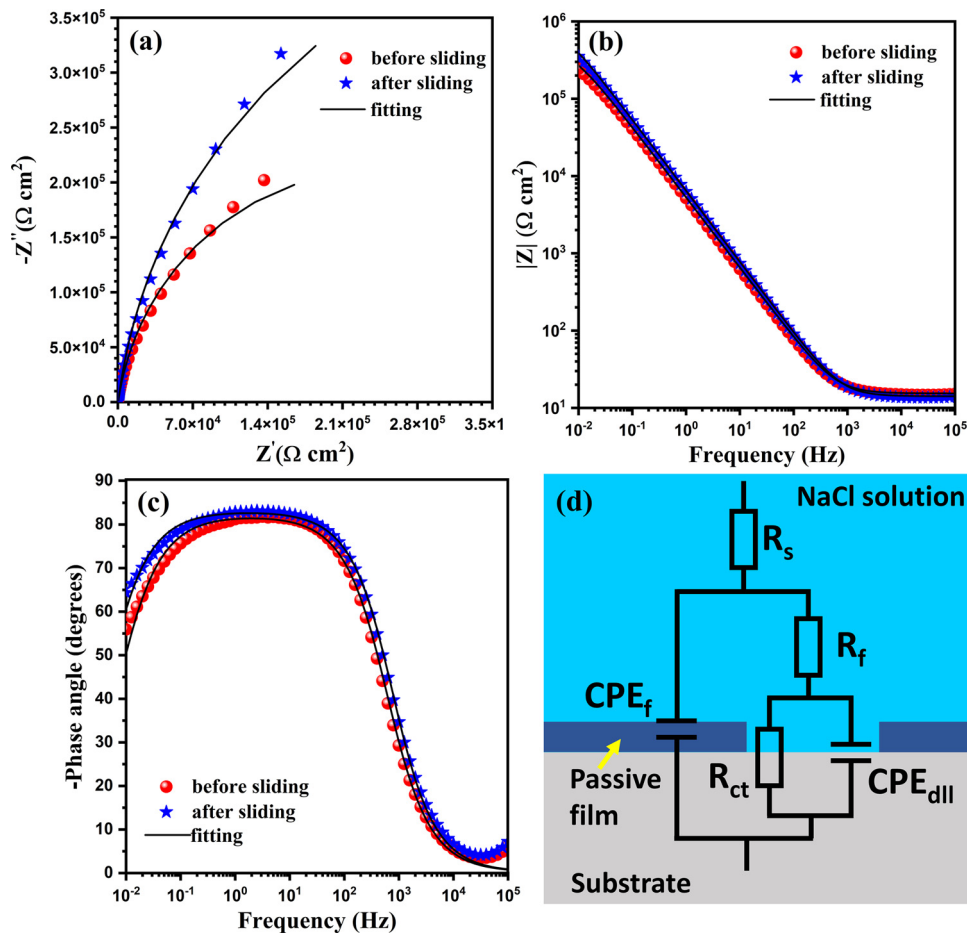
Fig. 12. EIS plots and fitted polarization resistance results of 316L SS before and after tribocorrosion test.
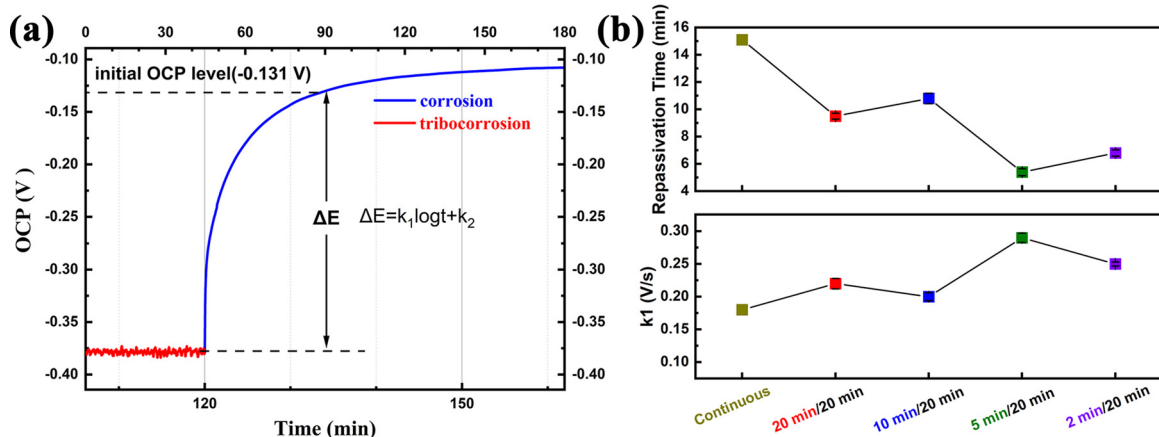

Fig. 13. Schemic illustration of evolution in OCP of 316L SS during and after sliding (a), the evolution of repassivation time and repassivation rate (K_1) obtained from Fig. 4 during the intermittent tribocorrosion.

accordingly, indicating that the change of anodic reaction kinetic accelerates the growth of passive film.

The kinetics of the passive film formation has also been studied by Okorie and Nowak [36] through the voltage-step technique, and the detected transient current can be described as the following equation:

$$i_t = i_{2D}\exp\left(-\frac{t}{\tau_{2D}}\right) + i_{3D}\left(-\frac{t}{\tau_{3D}}\right) + i_0 \tag{3}$$

In Eq. (3), the first term characterizes the nucleation kinetics of passive film (τ_{2D}) and the second term quantifies the passive

thickening rate (τ_{3D}): i_{2D} and i_{3D} are the detected current with time and the function of applied potential and film resistance performance. i_0 is introduced to consider the steady-state current of the passive film. After the sliding, the reformation of passive film is a complex process and the dominate mechanisms in different regions are different. The formation of passive film follows the following successions: (1) the nucleation of islands and lateral growth of these islands; (2) the initial rapid growth of a three-dimensional (3D) film with a worse density; (3) the continuous growth of film leading to a better density and thickening film; (4) thickening of
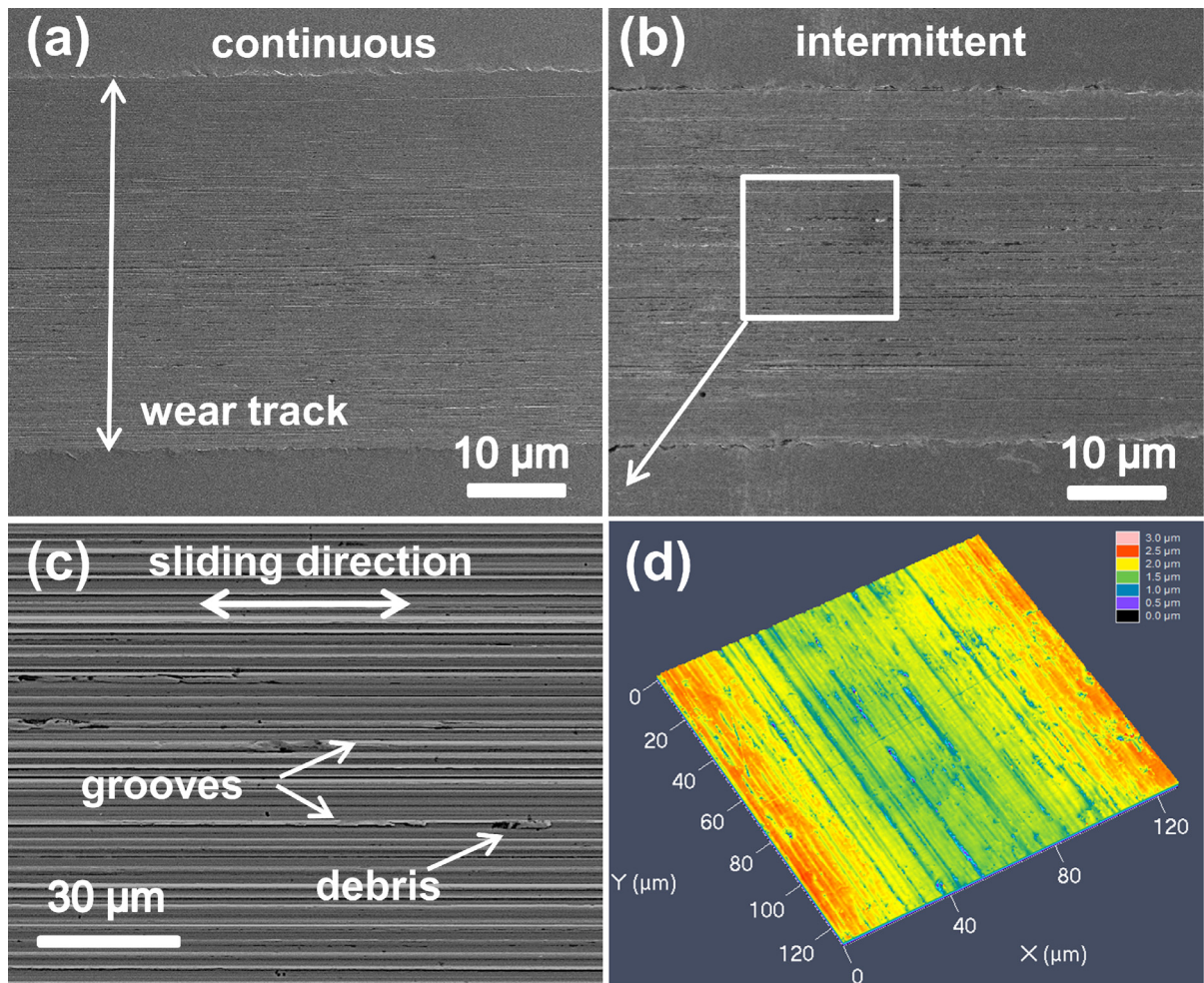
Fig. 14. SEM morphology of the wear track after continuous (a) and intermittent (b) tribocorrison test, local enlarged draw inside the wear track (c) and the 3D image of the wear track determined by laser optical profilometry (d), R_q=0.265 μm.

the denser passive film by a field-assisted diffusion mechanism [37,38]. Among these processes, the last process of thickening the passive film is the most time consuming and the former processes are relatively fast. Therefore, if the pause duration is larger than the required repassivation time, the measured data fit the logarithmic growth law, just as OCP response in Fig. 4. As a contrast, OCP cannot reverse back to the initial level with shortening the pause duration from 20 min to 5 min in Fig. 6. According to the analysis above, the shortage of pause duration in this experiment condition led to the reformed passive thin and porous, which causes a galvanic couple to exist in wear track, representing a lower OCP value. These discussions suggest that density and thickness of the reformed passive film inside wear track are strongly dependent on the pause duration time. The longer the pause duration is, the denser and thicker the reformed passive film is.

4.2. The microstructure evolution and transpassivation behavior

As one of the typical austenitic SSs, 316L (γ, face-centered cubic(fcc)) presents excellent corrosion resistance, but the contract stress-induced microstructure evolution during tribocorrosion is highly susceptible due to its relatively poor hardness. In this case, the initial contact pressure is much higher than that of yield strength of 316L SS, thus the deformation induced by frictional shear force can be easily observed under the wear track. As is well known, the deformation mechanism of fcc metals under cold work-

ing closely depends on their stacking fault energy (SFE), which depends on the alloy components and controls the formation of shear bands, and thus the nucleation site of the martensite [39]. Hence, SFE plays a critical role in determining whether twinning, martensite transformation or dislocation glide will dominate the deformation process of the material [40,41]. So far, it has been reported that there are two transformation mechanisms from austenite to martensite, i.e., stress-assisted martensite transformation, i.e., γ-austenite (fcc)$\rightarrow \varepsilon$ martensite (hexagonal-close-paged, hcp)$\rightarrow \alpha$'-martensite (bode-center-bcubic, bcc) and strain-induced martensite transformation, i.e., γ-austenite$\rightarrow$twining$\rightarrow \alpha$'-martensite. For 316L SS with SFE of ~40 mJ m^{-2}, twining is considered as dominant deformation mechanism since SFE at the range of 18–45 mJ m^{-2} [40]. From the cross-sectional images (Figs. 8 and 9), it can be found that some stripes present on deformed area after sliding. Beside, detailed TEM results further proved that the α'-martensite transformation has appeared. These results indicate that the deformation process follows the sequence of $\gamma \rightarrow$twining$\rightarrow \alpha$', which belongs to strain-induced transformation mechanism. Moreover, it should also be noted that the friction process is different from conventional cold working process, SFE would increase during the frictional shear force and make the deformation gradual from twining$\rightarrow \alpha$'-martensite towards dislocation slip under progressing strain [42].

Apparently, the transpassivation phenomenon, as evidenced by the recovered OCP, occurred both after the continuous and in-
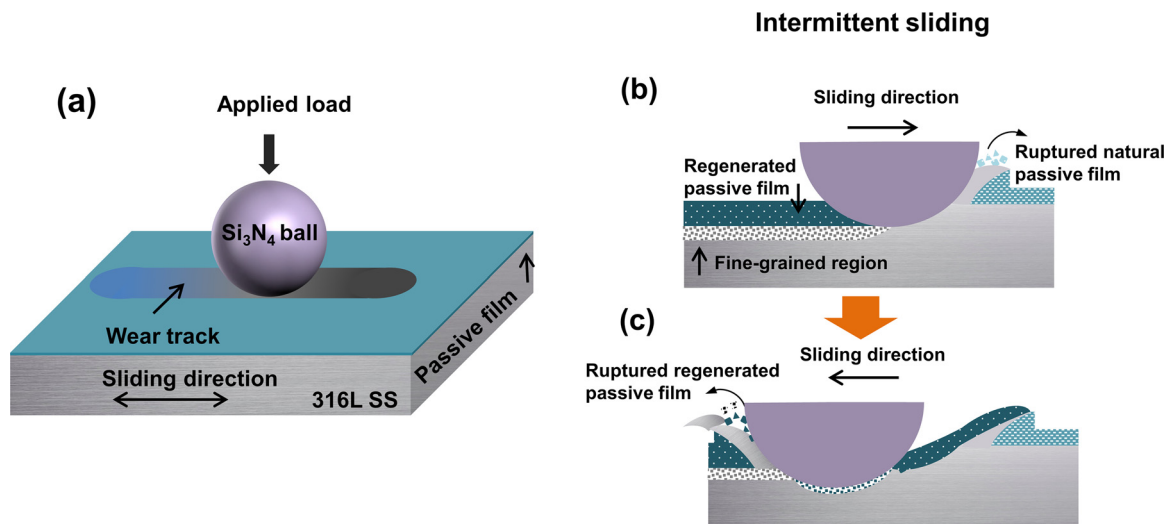
Intermittent sliding

Fig. 15. Schematic interactions of different wear track characteristics during the intermittent sliding process.

termittent sliding modes as long as pause duration is sufficient. The recovery of OCP after sliding characterized the ability of the growth of passive film inside a deformed wear track. Consequently, this is not only related to pause duration, but also microstructure evolution within the wear track [14]. For the passivated alloy or materials, its corrosion resistance is attributed to the dense and protective passive film formed on its surface, which acts as a barrier between the bare material and corrosive media. TEM observation (Fig. 9) clearly shows that the coarse structure has become binding and equiaxed grain structure with a size of 80 nm–200 nm after the sliding, where a dense dislocation forest surrounding the grain and darker bands can easily be distinguished. Apparently, the transpassivation behavior in the present study is induced by the microstructure inside the wear track once the other experiment conditions are kept the same. According to physical meaning of COP, the transpassivation behavior reflects an improved protection of the reformed passive film. EIS results (Fig. 12) clearly show that the electron transfer resistance increases by 46.7% after the sliding, demonstrating a significantly enhanced electrochemical stability of reformed passivate surface. In essence, the electrochemical stability reflects the resistance to electrochemical attack, which involves electron transfer at the interface between metal and corrosive media. Consequently, for a surface covered by a passive film, the degree of easing of the electron at the interface is related to the protective role of the reformed passive film. The chemical composition of a passive film in SS is mainly an oxide or hydroxide of Cr and Fe in SS, the distribution and diffusion of Cr is therefore the critical factor to affect the formation process and the protective property of the now passive film [43]. XPS results suggested that the passive films formed inside and outside the wear track have a similar structure which consists of layer constituting of $(Cr, Fe)_2O_3$. However, the reformed passive film inside the wear track presents an increased thickness after sliding. These results indicate that sliding treatment could result in nanocrystallization with the wear track, which is beneficial to the formation of a dense and a protective passive film. It is well known that the growth of passive film is affected by the microstructure of a passive alloy. Although some researches have indicated that decreasing the size of grain increases the density of diffusion paths for elements to migrate, the enhanced diffusion process is not considered to occur at room temperature in the present study [44]. On the contrary, the nanocrystallization increased the passivation rate through providing a more nucleation site, which is a better explanation for the improved passivated process in the present study [44]. In addition,

the influence of martensite phase transformation on the passive behavior after sliding was not discussed independently here because of the difficulty of separating the martensite transformation from grain refinement, dislocation structure and stress concentration on the corrosion behavior inside the wear track. Therefore, the transpassivation behavior and better corrosion resistance after the sliding are attributed to the nanocrystallization inside the wear track that promotes the formation of passive film and increases its thickness and compactness.

4.3. The accelerated mechanism under the intermittent tribocorrosion process

The wear rate (Figs. 5(b) and 7(b)) calculated from the two intermittent tribocorrosion modes shows that the sample which was conducted with the longest pause duration ($X = 20$ min) and the most sliding cycles ($Y = 2$ min, $n = 30$) produces the most significant deterioration of material loss. Microstructure evolution analysis proves that the nanocrystallizaion combined with sufficient pause duration promotes the thickness and compactness of a new-formed passive film inside the wear track after sliding. Consequently, the most sliding cycles combined with completely repassivated wear track led to the maximum material loss in the intermittent sliding. Apparently, the deteriorated tribocorrosion resistance is related to the formation and removal of the passive film inside the wear track. Previous studies have found that the wear rate during the tribocorrosion tests was closely related to the presence or not of a passive film in the contact area [45,46]. Hard and brittle solid passive oxide films are considered as third body particles or transfer film within the sliding contact area, which involves an a ductile metal (first body) and a hard inert counterpart (second body) [47].

Fig. 14 presents the morphological characteristics of the wear track under two sliding modes. It is clear that the wear track morphology images are characterized by a relatively smooth and finer scratches after the continuous sliding, but the wider and deeper scratches present under the intermittent sliding (Fig. 14 (a, b)). This clearly indicates that the intermittent sliding produces a stronger abrasive wear on a smooth 316L SS surface. Due to the abrasive wear, the isolated and parallel grooves present on the whole contact surface. The material was smeared out inside the grooves and large plastically deformed ridges present on the surface (Fig. 14(c)), showing a typical 3-body abrasion characteristic.

According to OPC evolution, it can be deduced that the sliding contact area under the continuous sliding is in an active surface state, while it changes within sliding time under the intermittent sliding. That is, the wear track alternates between the active and repassivated state during each cycle under the intermittent sliding. Owing to the refinement of grains within the wear track, the regenerated passive film is more compact and thicker during the pause duration. Then these passive films will be scratched in the subsequence sliding process. Beside, the hardened substrate due to the phase transformation inside the wear would also be ejected and act as hard abrasive particles. Consequently, the spalling of the repassivated film or hardened substrate was ejected and caused deeper abrasive stretches.

However, it should be noted that the material loss is caused by not only the abrasive wear, but also by the electrochemical corrosion of the metal. The active state at the wear track under the continuous sliding undergoes a chemical dissolution, which releases free metal ions to solution. The active-passivate alternate transition during the intermittent sliding leads to the release of both partial free metal ions and solid passive film from the substrate, which accelerates the material loss. According to the above analysis, the enhanced deteriorated mechanism of material loss is schematically presented in Fig. 15.

Therefore, it can be illustrated that in the present study the accelerated deterioration of material loss during the intermittent tribocorrosion is attributed to the severer and more repetitive abrasive wear, whose periodicity mechanically removes the thickened and denser passive film inside the wear track.

5. Conclusions

In this research, a comparative study on tribocorrosion behavior of 316L SS under continuous and intermittent slidings was conducted. Compared with the continuous sliding, the material loss was enhanced under the intermittent sliding as the friction surface was repassivated after sliding. It was found that due to the repeated mechanical slidings, a plastically deformed layer occurred underneath the wear track. Grain refinement and martensite transformation ($\gamma \rightarrow$ twining $\rightarrow \alpha$') were clearly observed in the deformation layer. This microstructure evolution not only improves the mechanical properties inside the wear track, but also promotes the formation of a thicker and compact passive film. Therefore, repeated removal of the thickened and hard solid passive film from the repassivated wear track significantly enhances the abrasive wear during the intermittent sliding, which causes greater material loss as compared with the continuous sliding.

Data availability statement

The data used to support the findings of this study are available from the corresponding authors upon request.

Declaration of Competing Interest

The authors declare that they have no known competing financial interests or personal relationships that could have appeared to influence the work reported in this paper.

CRediT authorship contribution statement

Yingrui Liu: Methodology, Investigation, Validation, Writing – original draft. **Linlin Liu:** Conceptualization, Methodology, Investigation, Validation. **Shuyu Li:** Methodology, Investigation. **Rujia Wang:** Methodology, Investigation. **Peng Guo:** Visualization. **Aiying Wang:** Writing – review & editing, Funding acquisition, Supervision. **Peiling Ke:** Writing – review & editing, Supervision, Funding acquisition.

References

[1] R.J.K. Wood, Wear 376-377 (2017) 893–910.
[2] J. Chen, J. Wang, F. Yan, Q. Zhang, Q.A. Li, Tribol. Int. 81 (2015) 1–8.
[3] F.B. Saada, Z. Antar, K. Elleuch, P. Ponthiaux, Wear 328-329 (2015) 509–517.
[4] F.B. Saada, Z. Antar, K. Elleuch, P. Ponthiaux, N. Gey, Wear 394-395 (2018) 71–79.
[5] M.K. Dimah, F. Devesa Albeza, V. Amigó Borrás, A. Igual Muñoz, Wear 294-295 (2012) 409–418.
[6] R. Yazdi, H.M. Ghasemi, C. Wang, A. Neville, Corros. Sci. 128 (2017) 23–32.
[7] M.T. Mathew, M.A. Wimmer, Tribocorrosion of Passive Metals and Coatings, 2011, pp. 368–400.
[8] A. López-Ortega, J.L. Arana, R. Bayón, Int. J. Corros. 2018 (2018) 1–24.
[9] Y. Zhang, X. Yin, J. Wang, F. Yan, Corros. Sci. 88 (2014) 423–433.
[10] F. Toptan, A.C. Alves, I. Kerti, E. Ariza, L.A. Rocha, Wear 306 (2013) 27–35.
[11] V.G. Pina, V. Amigó, A.I. Muñoz, Corros. Sci. 109 (2016) 115–125.
[12] Z. Doni, A.C. Alves, F. Toptan, J.R. Gomes, A. Ramalho, M. Buciumeanu, L. Palaghian, F.S. Silva, Mater. Des. 52 (2013) 47–57 (1980-2015).
[13] S. Mischler, S. Debaud, D. Landolt, J. Electrochem. Soc. 145 (1998) 750–758.
[14] V. Dalbert, N. Mary, B. Normand, C. Verdu, T. Douillard, S. Saedlou, Wear 420-421 (2019) 245–256.
[15] S. Jelliti, C. Richard, D. Retraint, T. Roland, M. Chemkhi, C. Demangel, Surf. Coat. Technol. 224 (2013) 82–87.
[16] J. Li, Y.H. Lu, X.H. Tu, W. Li, Wear 414-415 (2018) 289–295.
[17] J. Perret, E. Boehm-Courjault, M. Cantoni, S. Mischler, A. Beaudouin, W. Chitty, J.P. Vernot, Wear 269 (2010) 383–393.
[18] B. Zhang, J. Wang, F. Yan, Corros. Sci. 131 (2018) 252–263.
[19] M. Salasi, G. Stachowiak, G. Stachowiak, Corros. Sci. 98 (2015) 20–32.
[20] R.C.C. Silva, R.P. Nogueira, I.N. Bastos, Electrochim. Acta 56 (2011) 8839–8845.
[21] Y. Sun, E. Haruman, Surf. Coat. Technol. 205 (2011) 4280–4290.
[22] C.B. von der Ohe, R. Johnsen, N. Espallargas, Wear 269 (2010) 607–616.
[23] Q. Guo, J. Liu, M. Yu, S. Li, Appl. Surf. Sci. 327 (2015) 313–320.
[24] D. Wu, Z. Guan, Q. Cheng, W. Guo, M. Tang, Y. Liu, Wear 452-453 (2020) 203294.
[25] I. Çaha, A.C. Alves, C. Chirico, S.A. Tsipas, I.R. Rodrigues, A.M.P. Pinto, C.R. Grandini, L.A. Rocha, E. Gordo, F. Toptan, Corros. Sci. 176 (2020) 108925.
[26] P. Ponthiaux, F. Wenger, D. Drees, J.P. Celis, Wear 256 (2004) 459–468.
[27] A. López, R. Bayón, F. Pagano, A. Igartua, A. Arredondo, J.L. Arana, J.J. González, Wear 338-339 (2015) 1–10.
[28] A.C. Vieira, L.A. Rocha, N. Papageorgiou, S. Mischler, Corros. Sci. 54 (2012) 26–35.
[29] A. Ahmadi, F. Sadeghi, J. Tribol. Trans. ASME 143 (2021) 14.
[30] L. Li, L.L. Liu, X. Li, P. Guo, P. Ke, A. Wang, ACS Appl. Mater. Interfaces 10 (2018) 13187–13198.
[31] D. Klotz, Electrochem. Commun. 98 (2019) 58–62.
[32] N. Mary, B. Ter-Ovanessian, B. Normand, Wear 460-461 (2020) 23478–23488.
[33] S. Kossman, L.B. Coelho, A. Mejias, A. Montagne, A. Van Gorp, T. Coorevits, M. Touzin, M. Poorteman, M.G. Olivier, A. Iost, M.H. Staia, Wear 456-457 (2020) 203341–203355.
[34] M. Keddam, F. Wenger, D. Landolt, S. Mischler, in: Tribocorrosion of Passive Metals and Coatings, Woodhead Publishing, 2011, pp. 187–221.
[35] T. Hanawa, K. Asami, K. Asaoka, J. Biomed. Mater. Res. 40 (1998) 530–538.
[36] B.A. Okorie, W.B. Nowak, J. Electrochem. Soc. 130 (1983) 290–296.
[37] K. Fushimi, T. Yamamoto, K. Azumi, M. Seo, H. Habazaki, Electrochim. Acta 52 (2007) 6901–6910.
[38] P. Jemmely, S. Mischler, D. Landolt, Wear 237 (2000) 63–76.
[39] S. Wei, H. Zhang, J. Tangpatjaroen, J. Tarnsangpradit, A.D. Usta, M. Eriten, J.H. Perepezko, I. Szlufarska, Acta Mater. 209 (2021) 116787.
[40] C.C. Bampton, I.P. Jones, M.H. Loretto, Acta Metall. 26 (1978) 39–51.
[41] Y.F. Shen, X.X. Li, X. Sun, Y.D. Wang, L. Zuo, Mater. Sci. Eng A 552 (2012) 514–522.
[42] S.S.F. de Dafé, D.R. Moreira, M.d.S. Matoso, B.M. Gonzalez, D.B. Santos, Mater. Sci. Forum 753 (2013) 185–190.
[43] M. Benoit, C. Bataillon, B. Gwinner, F. Miserque, M.E. Orazem, C.M. Sánchez-Sánchez, B. Tribollet, V. Vivier, Electrochim. Acta 201 (2016) 340–347.
[44] X.Y. Wang, D.Y. Li, Electrochim. Acta 47 (2002) 3939–3947.
[45] P. Henry, J. Takadoum, P. Berçot, Corros. Sci. 51 (2009) 1308–1314.
[46] R. Priya, C. Mallika, U.K. Mudali, Wear 310 (2014) 90–100.
[47] S. Mischler, A. Spiegel, D. Landolt, Wear 225-229 (1999) 1078–1087.